Earthquake Geology Field Guide

March 24, 2023

From the San Andreas Fault to the Ridgecrest ruptures

Prepared by

Krittanon “Pond” Sirorattanakul

Guanli Wang

Jean-Philippe Avouac

Geomechanics and Mitigation of Geohazards (GMG)

California Institute of Technology

Tentative Schedule

7.00 am: depart Caltech; drive 1 hr 10 mins
8.10 am: arrive at Stop 1 (Palmdale roadcut); 30 mins
8.40 am: depart from Stop 1; drive 40 mins
9.20 am: arrive at Stop 2 (Lake Elizabeth Picnic Site); 35 mins; 15 mins *restroom break*
10.10 am: depart from Stop 2; drive 15 mins
10.25 am: arrive at Stop 3 (Fault gouge); 10 mins
10.35 am: depart from Stop 3; drive 15 mins
10.50 am: arrive at Stop 4 (Neenach volcano); 10 mins
11.00 am: depart from Stop 4; drive 1 hr
12.00 pm: arrive at Stop 5 (Garlock fault) near Shell (601 California City Blvd., Mojave – 10 mins further north of downtown Mojave); 45 mins including *restroom break* and *lunch*
12.45 pm: depart from Stop 5; drive 1 hr 15 mins
2.00 pm: arrive at Stop 6 (Ridgecrest ruptures); 45 mins
2.45 pm: depart from Stop 6; drive 1 hr 15 mins
4.00 pm: arrive at Chevron (15764 Sierra Hwy, Mojave); 20 mins *restroom break*
4.20 pm: depart Ridgecrest; drive 2 hr to Caltech or optionally stop 7
6.20 pm: arrive at Caltech or optionally Stop 7 (Lacy park); 25 mins
6.45 pm: depart from Stop 7; drive 15 mins
7.00 pm: arrive at Caltech

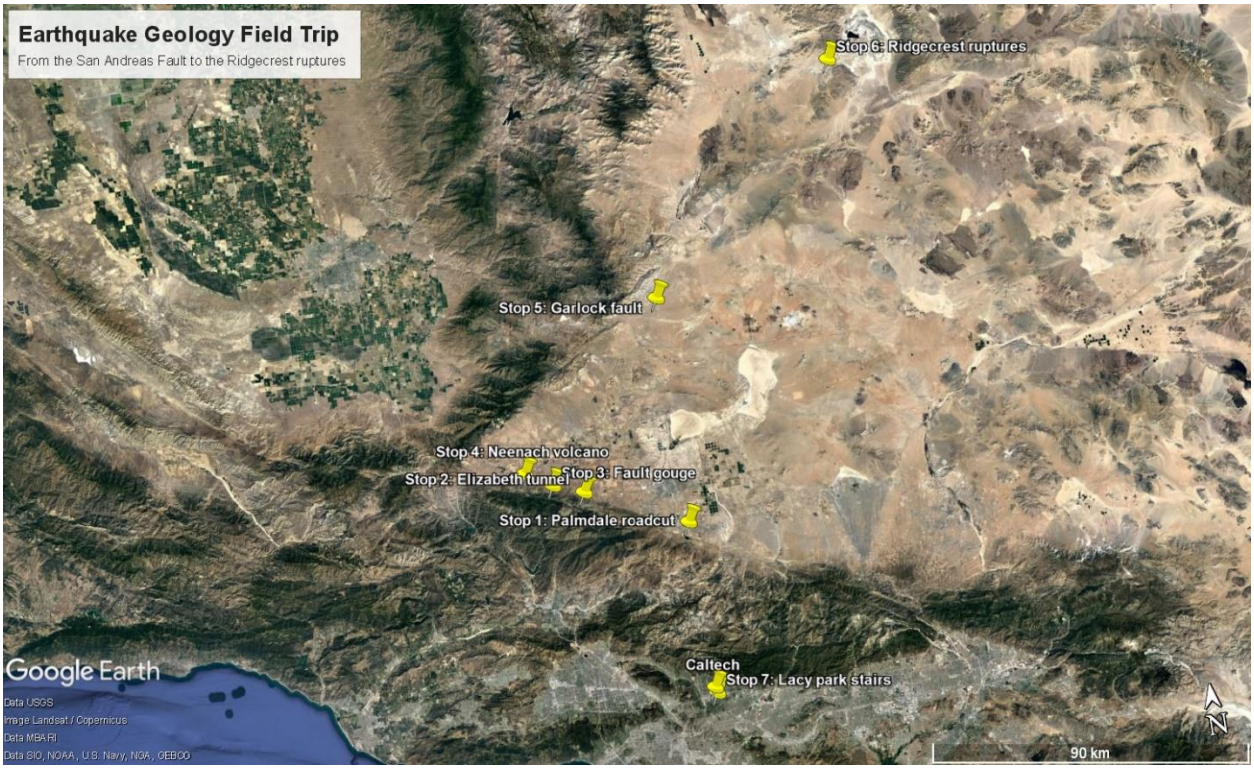

Stop 1: Palmdale roadcut (34.558104°N, 118.127890°W)

Complex folding and faulting related to the motion of the San Andreas fault can be found along the Hwy 14 roadcut near Palmdale, California. The roadcut is approximately 27 meters high and 600 meters long. Lower to middle Pliocene, gypsiferous, lacustrine rocks of the Anaverde Formation are overlain by a thin layer of undeformed Pleistocene.

The deformation in this roadcut is associated to the San Andreas fault (SAF). The SAF borders the North American and the Pacific plates and accommodate primarily right-lateral strike-slip motion up to 35 mm/yr. Two largest earthquakes in recent history of the western United States occurred along the SAF: the 1857 M7.9 Fort Tejon and the 1906 M7.9 San Francisco earthquakes. In between the two past ruptures exist the creeping section with creep rates up to 25 mm/yr. The southern-most portion near the Salton trough has not been ruptured for at least 320 years and has little seismic activity making it a good candidate for the next big one. It is projected that a magnitude 7.8 event initiated in the Salton trough could result in $200 billion of economic losses due to damages of buildings, fires, and disruption of water pipelines and telecommunications.

Figure 1.1. Palmdale roadcut (Photo by Pond Sirorattanakul).

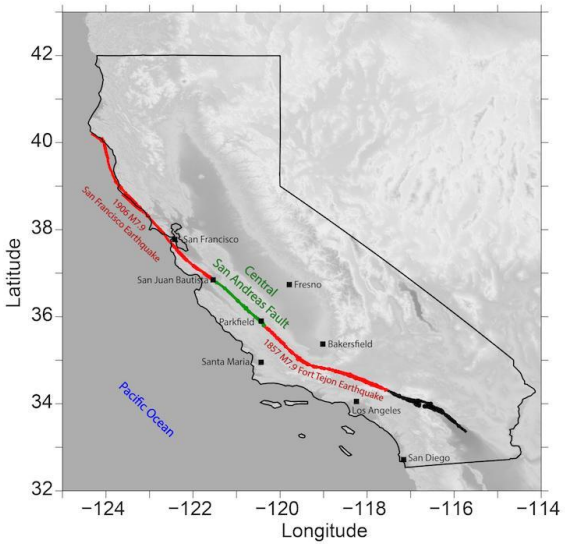

Figure 1.2. Historical earthquakes along the San Andreas Fault (SAF). Figure is from https://seismo.berkeley.edu/blog/2018/06/19/when-creep-becomes-unsteady.html

Besides the main strand of the SAF, there exist other multiple subsidiary fault strands, including the Little Rock fault. Fold axis and the strike of the faults (fault E in particular) are consistent with Riedel shear.

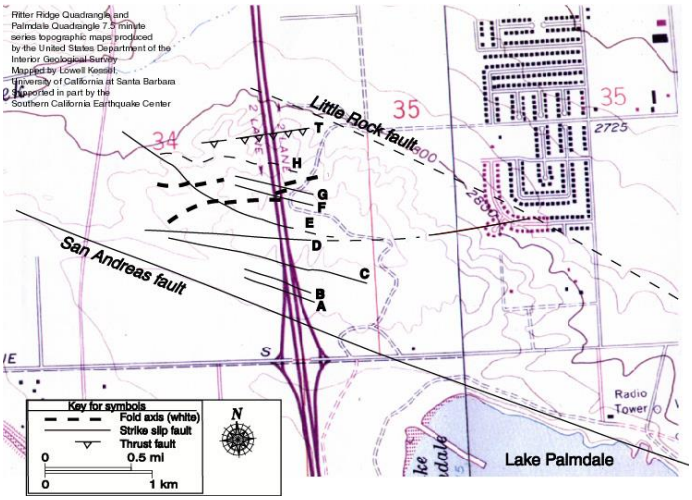

Figure 1.3. Structural map of faults and folds at the Palmdale roadcut by Lowell Kessel.

Principal stresses: $\sigma_1 > \sigma_2 > \sigma_3$

For strike-slip faults, σ_2 are always vertical. The direction perpendicular to σ_1 would be an axis of a fold, while the direction perpendicular to σ_3 would be the tension fractures that could develop into a Riedel shear.

The larger-scale tension fractures can develop into depressions or “pull-apart basins”. If it is filled with water, a sag pond can be created.

The folds can develop into “push-up ridges”. They could potential rotate to be in the direction parallel to the fault strand and create “shutter ridges”.

Keep in mind these features as we traverse along the SAF as we can spot many on the road.

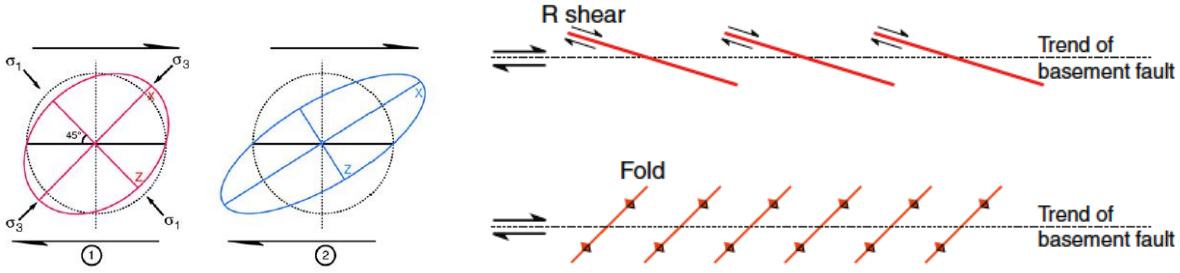

Figure 1.4. Concept of Riedel shear. A diagram for right-lateral strike-slip fault.

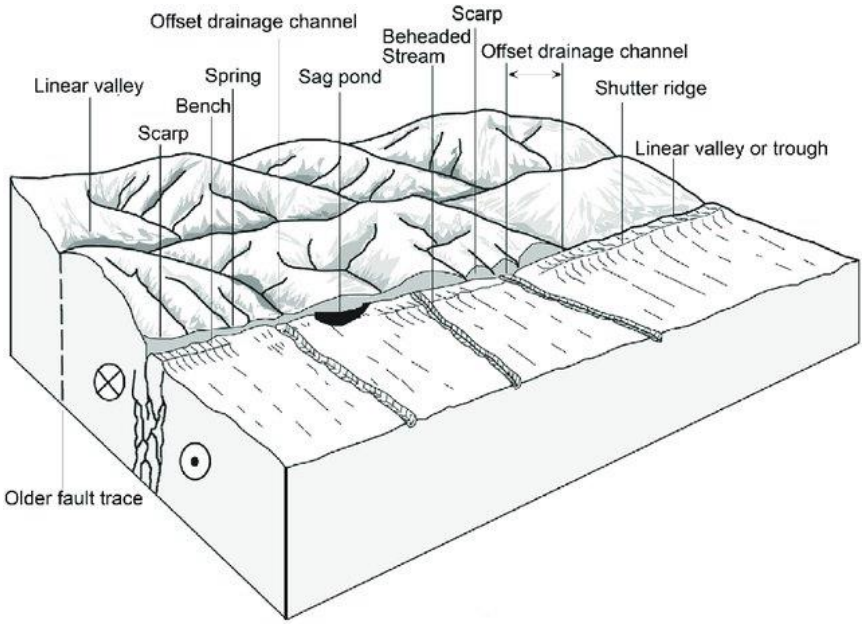

Figure 1.5. Morphotectonics of strike-slip faults.

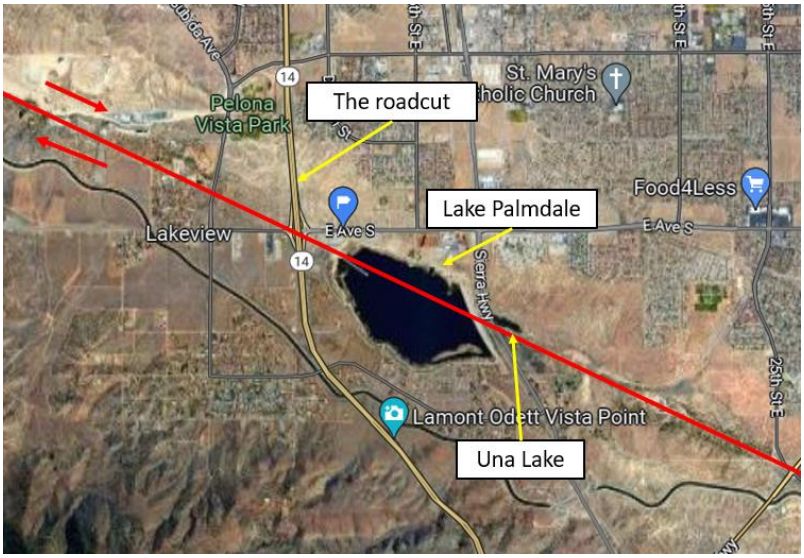

Figure 1.6. Una Lake is a natural sag pond occurring from the infill of rainfall in the depressions associated to the movement of the SAF. It used to be much larger and include the eastern area of the modern anthropogenic Lake Palmdale reservoir.

Further readings

Burbank. D. W. & Anderson, R. S. (2011), *Tectonic geomorphology*, John Wiley & Sons, Hoboken.

Jolivet, R., Simons, M., Agram, P. S., Duputzel, Z., & Shen, Z.-K. (2015), Aseismic slip and seismogenic coupling along the central San Andreas Fault, Geophysical Research Letters, 42, 297-306.

Rockwell, T., Scharer, K., & Dawson, T. (2016). Earthquake geology and paleoseismology of major strands of the San Andreas fault system. In *Applied geology in California* (Vol. 26). Association of Environmental and Engineering Geology Special Publication.

Stop 2: Lake Elizabeth picnic site (34.668736°N, 118.409773°W)

The Elizabeth tunnel is a segment of the Los Angeles aqueduct which channels water from the Owens Valley to the city of Los Angeles. It runs across the San Andreas Fault (SAF) at approximately 90 meters beneath the surface. In 1857, about half a century before the tunnel was built, an M7.9 Fort Tejon earthquake shook the area rupturing from Parkfield to Wrightwood. It is hence of interest to consider the problem of potential damage of the tunnel due to the next earthquakes.

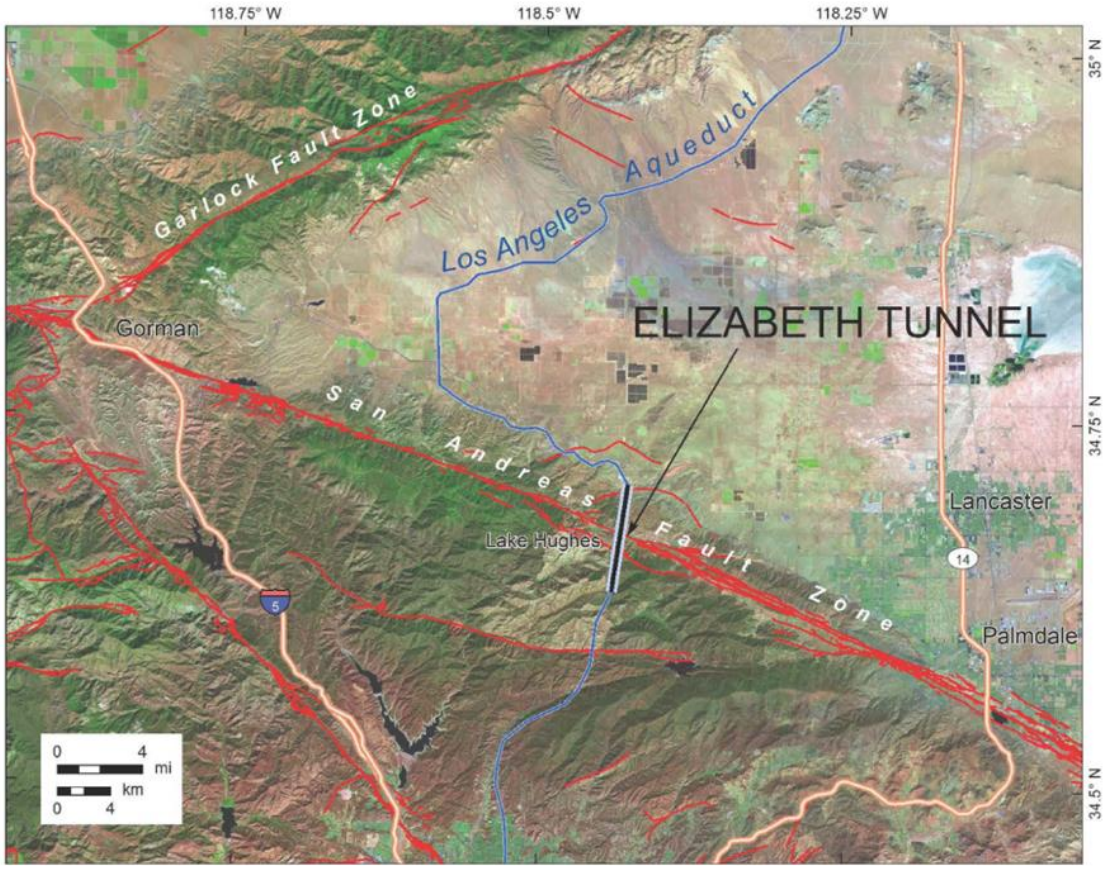

Figure 2.1. LA aqueduct crossing the San Andreas Fault at Elizabeth tunnel. Figure from Lindvall et al. (2017).

A simple framework can be adopted to evaluate the probability of malfunction, with a few assumptions made to simplify the calculations:

- damage of the tunnel within a given time period (e.g. the next 30 years) is considered as a random event and equivalent with having the cumulative slip caused by earthquakes exceeding a critical threshold, e.g., the width/diameter of the tunnel

- slip in an individual earthquake is assumed to follow a typical distribution, which could be empirically estimated from measurements of offsets of other regional earthquake sequences such as the 2019 Ridgecrest sequence (assuming ergodicity)
- the occurrence of earthquakes along the San Andreas fault (SAF) is assumed to be Poissonian and of the same magnitude and can be constrained using a simple moment balance from the 1857 Fort Tejon earthquake and the long-term slip rate
- a scaling law between moment and mean slip is assumed so that estimates from the Ridgecrest sequence are transferable to potential earthquakes along the SAF

In this case, Gamma distribution is chosen to characterize slip due to its mathematical convenience in the scale parameter and the simple form of obtaining the distribution of sums. The final probabilities of exceedance are hence calculated for different thresholds and durations of interest considering all possible combinations of earthquake occurrence and slip.

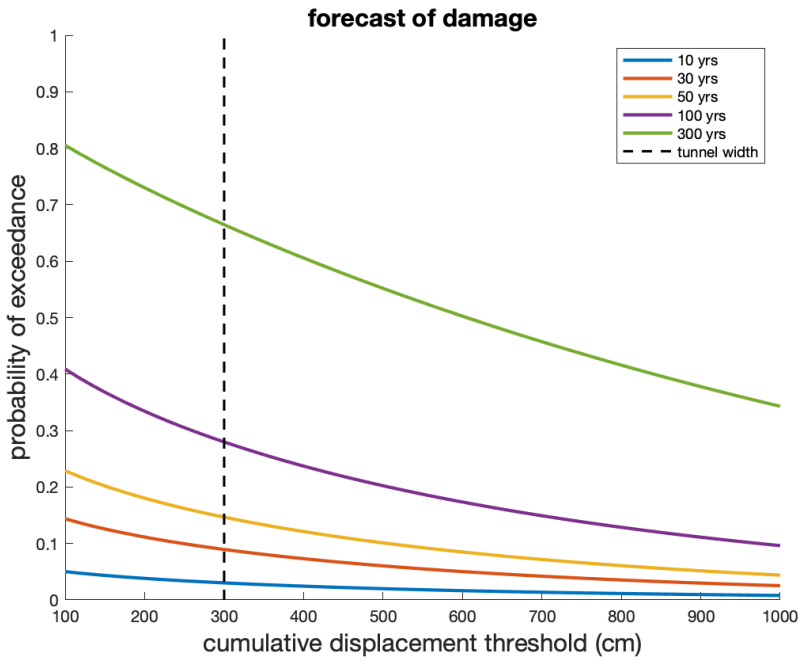

Figure 2.2. Simple forecast of cumulative displacement across the San Andreas Fault at the Elizabeth tunnel (Guanli Wang).

Further readings

Lindvall, S. C., Kerwin, S., Evans, J. P., Tyson, J., Chestnut, J., Heron, C., Mass, K., Scharer, K. M., McPhillips, D., Moore, D., Farr, M., Ballard, C., Williams, R. T., Bradbury, K. K., Rowe, C. D., & Savage, H. M. (2017, 08). San Andreas Fault Characterization at the LADWP Elizabeth Tunnel. Poster Presentation at 2017 SCEC Annual Meeting.

Ponti, D. J. et al. (2020), Documentation of surface fault rupture and ground-deformation features produced by the 4 and 5 July 2019 MW 6.4 and MW 7.1 Ridgecrest earthquake sequence, *Seismological Research Letters*, *91*(5), 2942–2959.

Stop 3: Fault gouge (34.701503°N, 118.520891°W)

The grinding of the two sides of the fault produce tiny powders commonly referred to as “fault gouge”. They form from localization of strain within the fault zone under brittle conditions near the earth’s surface. In this stop, a patch of fault gouge is exposed on the outcrop along Pine Canyon road, stretching over 500 meters.

Figure 3.1. Fault gouge along the San Andreas Fault near Three Points, CA (Photo by Pond Sirorattanakul).

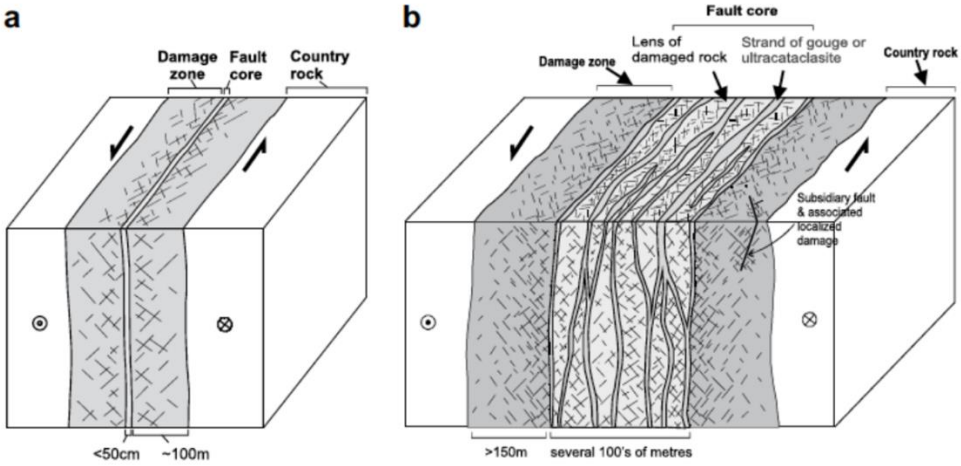

Figure 3.2. Models of the internal structure of fault zones at different scales (Mitchell and Faulkner, 2009).

Further reading

Mitchell, T. M. & Faulkner, D. R. (2009), The nature and origin of off-fault damage surrounding strike-slip fault zones with a wide range of displacements: A field study from the Atacama fault system, northern Chile, *Journal of Structural Geology*, 31(9), 802-816.

Stop 4: Neenach volcano (34.740928°N, 118.599710°W)

The Neenach volcanics section composed primarily of rhyolites deeply resembles that of the volcanics in the Pinnacle National Park. Quantitative geochronology dates both of them to approximately 23 million years old. Their petrographic textures are also remarkably similar. With the distances of 315 km apart from one another, it implies average relative slip rate along the San Andreas Fault to be approximately 15 mm/yr.

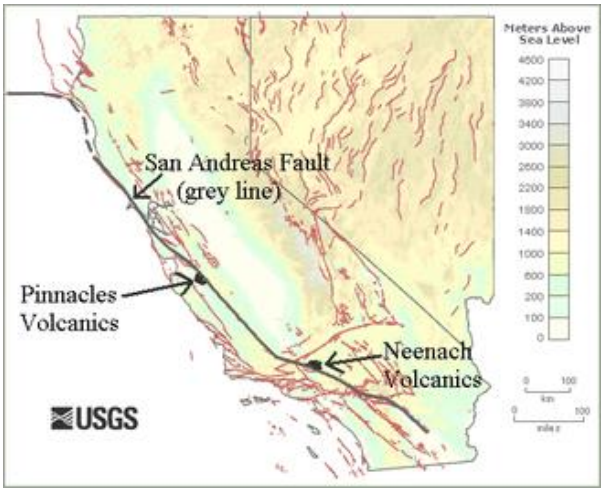

Figure 4.1. Correlations between Neenach and Pinnacles.

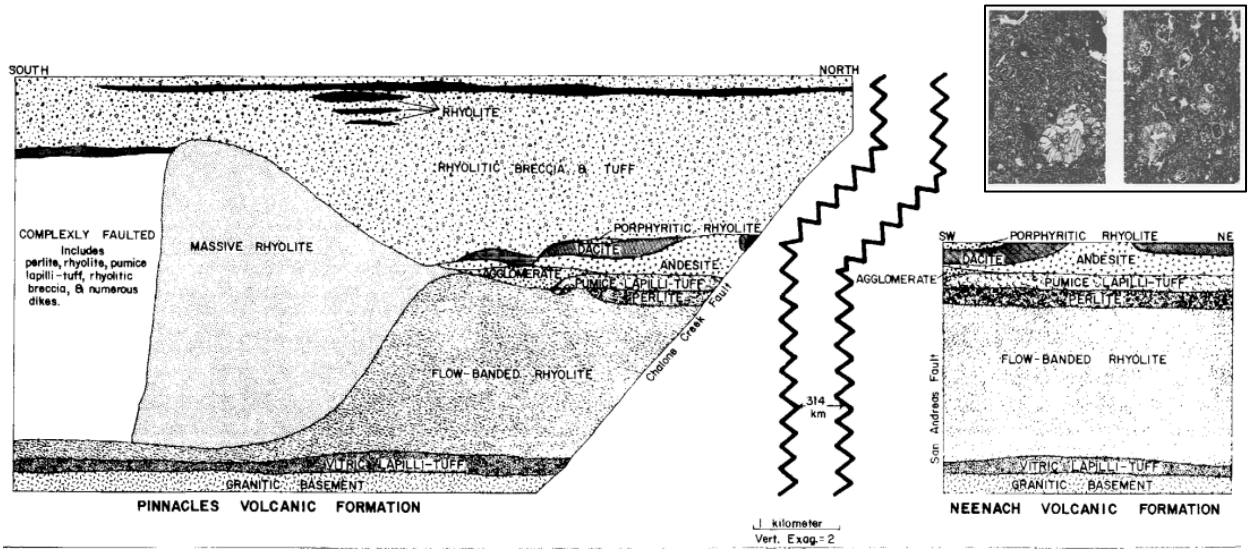

Figure 4.2. Geological cross-sections and petrographic similarity of augite-olivine andesite from Pinnacles (left) and Neenach volcanics (right). Figure is from Matthews (1976).

Further reading

Matthews, V. (1976), Correlation of Pinnacles and Neenach Volcanic formations and their bearing on San Andreas fault, *AAPG Bulletin*, 60, 2128-2141.

Stop 5: Garlock fault (35.125648°N, 118.117928°W)

Garlock fault is one of the most prominent geological lineation in southern California. Based on paleoseismology, the fault is predominantly left-lateral strike-slip and accommodates the strain between the extensional tectonics of the Great Basin and the right-lateral strike-slip faulting of the Mojave Desert. Little seismicity and little surface displacements were detected in the modern history. However, following large earthquakes, such as the 1992 Landers earthquake or the 2019 Ridgecrest earthquakes, the faults have seen to show some seismic swarms and shallow aseismic creep. The seismic hazard assessment of the fault is difficult and remains largely unconstrained.

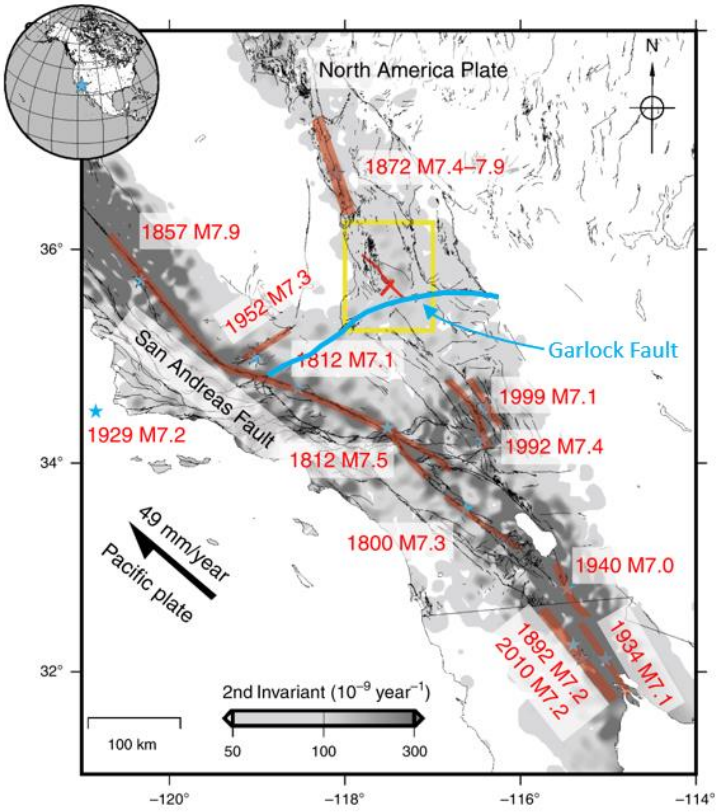

Figure 5.1. Strain rate accumulation in southern California inferred from geodetic measurements. Adapted from Chen et al. (2020).

Further readings

Chen, K., Avouac, J.-P., Aati, S., Milliner, C., Zheng, F., & Shi, C. (2020). Cascading and pulse-like ruptures during the 2019 Ridgecrest earthquakes in the eastern California shear zone. Nature Communications, 11, 22.

McGill, S. and Sieh, K. (1993), Holocene slip rate of the Central Garlock Fault in southeastern Searles Valley, California, *Journal of Geophysical Research*, 98(B8), 14217-14231.

Ross, Z. E., Idini, B., Zhe, J., Stephenson, O. L., Zhong, M., Xin, W., Zhan, Z., Simons, M., Fielding, E. J., Yun, S.-H., Hauksson, E., Moore, A. W., Liu, Z., Jung, J. (2019), Hierarchical interlocked orthogonal faulting in the 2019 Ridgecrest earthquake sequence, *Science*, 366, 346-351.

Stop 6: Ridgecrest ruptures (35.649254°N, 117.475054°W)

The Ridgecrest earthquake sequence starts with a M_w 6.4 foreshock on July 4th, 2019 followed by a M_w 7.1 mainshock 34 hours later. To date, this is probably one of the most well-studied and well-documented earthquake sequences with abundant seismic, geodetic, and field data. The foreshock ruptured two orthogonal faults, while the mainshock mostly ruptured the main NW-SE fault. Many morphotectonic features of a strike-slip fault such as the Riedel shear can be observed in the field. There is also evidence of rocks that got thrown out of place suggesting that the peak ground acceleration could be as large as 1g in the near-field. Continuous recording GNSS stations show the evolution from a crack rupture to a slip-pulse rupture. The absence of aftershocks around the Coso geothermal field suggest that the elastic stresses were locally depleted by the geothermal operations.

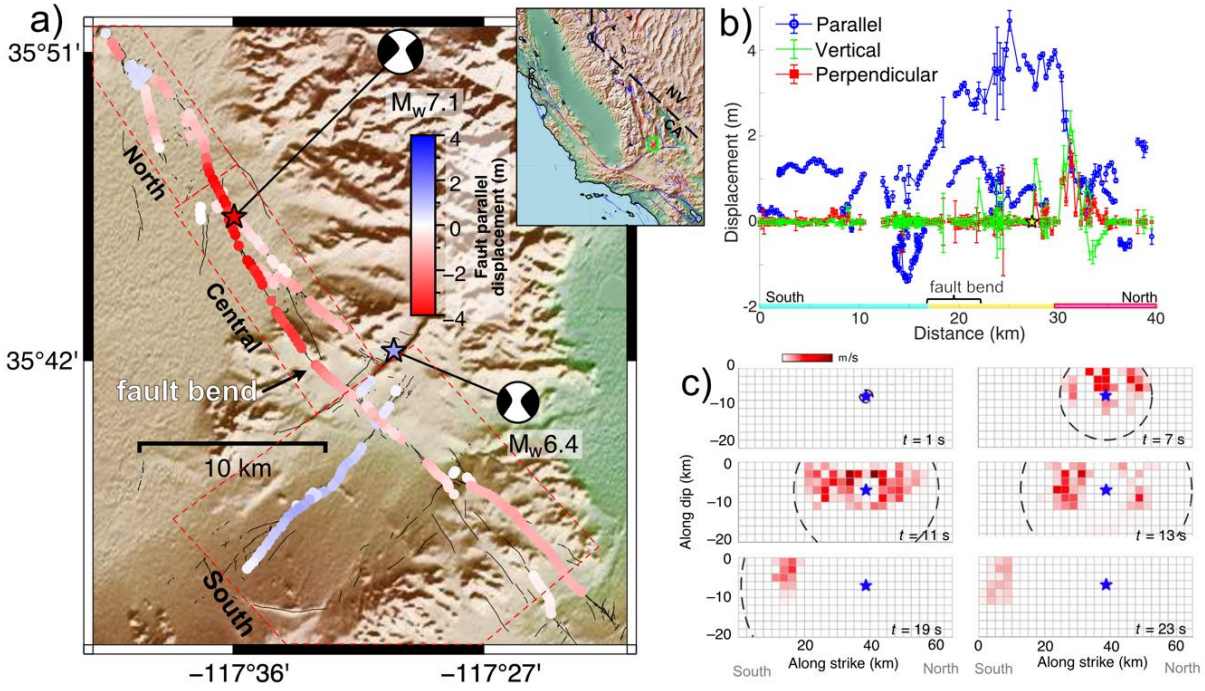

Figure 6.1. The Ridgecrest earthquake sequences. Surface ruptures measured from optical image correlation and kinematic of the rupture during the mainshock derived from the inversion of the high rate GNNS records and remote sensing (Chen et al., 2020).

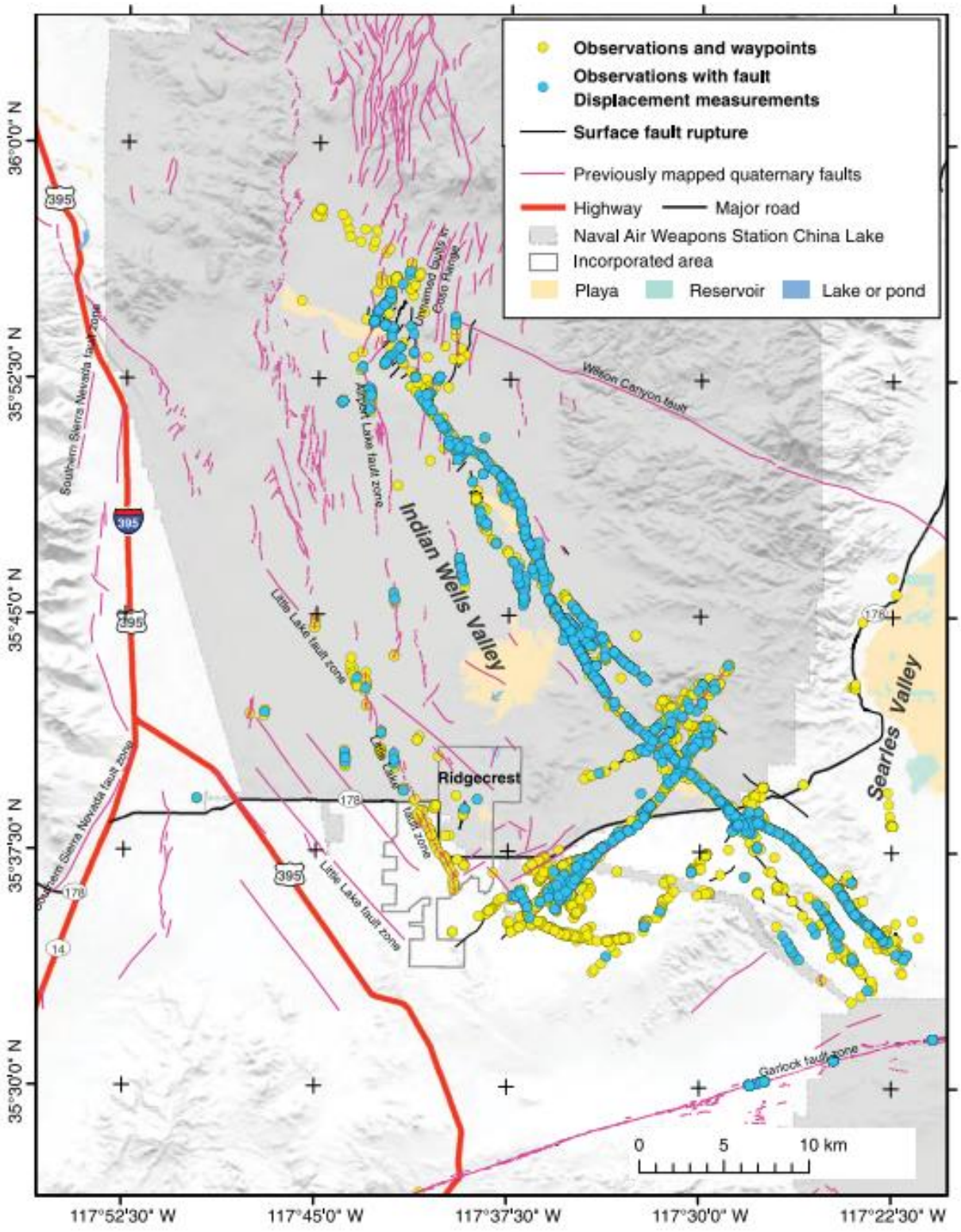

Figure 6.2. Locations with surface field measurements. Figure from Ponti et al. (2020).

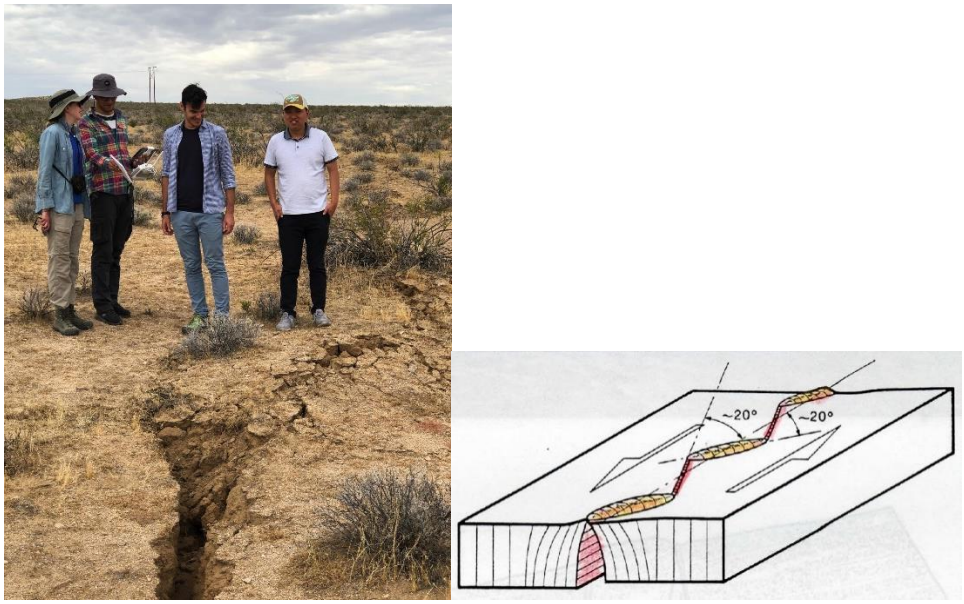

Figure 6.3. An example of a Riedel shear observed at the Ridgecrest ruptures. (Photo and drawing from Jean-Philippe Avouac)

Figure 6.4. An example of a rock that got thrown out of place during the earthquake. Figure is from Hough et al. (2020).

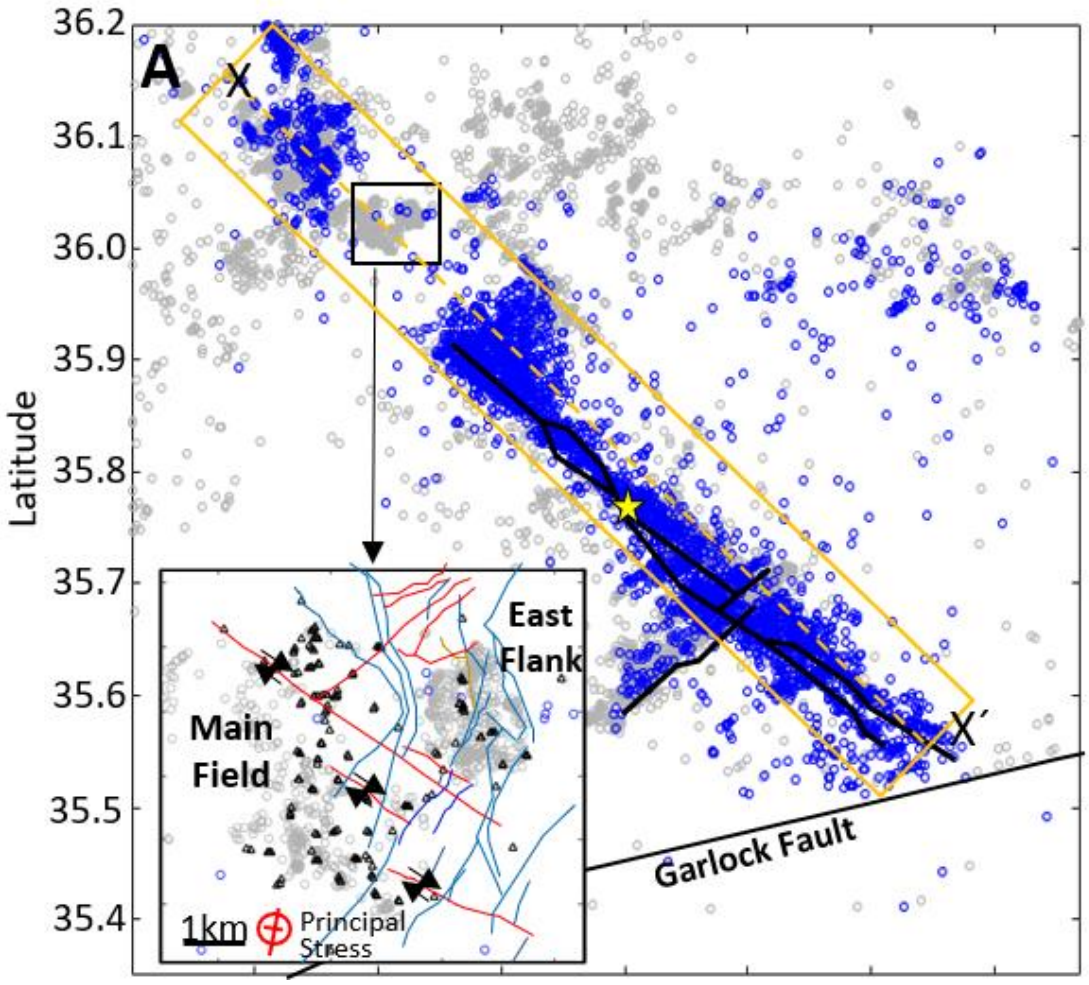

Figure 6.5. Aftershocks of the 2019 Ridgecrest earthquakes. Note the absence of aftershocks, probably due to geothermal project at Coso geothermal field (Chen et al., 2020).

Further readings

Chen, K., Avouac, J.-P., Aati, S., Milliner, C., Zheng, F., & Shi, C. (2020), Cascading and pulse-like ruptures during the 2019 Ridgecrest earthquakes in the eastern California shear zone. Nature Communications, 11, 22.

Hough, S. E., Thompson, E., Parker, G. A., Graves, R. W., Hudnut, K. W., Patton, J., Dawson, T., Ladinsky, T., Oskin, M., Sirorattanakul, K., Blake, K., Baltay, A., Cochran, E. (2020), Near-field ground motions from the July 2019 Ridgecrest, California, earthquake sequence, *Seismological Research Letters,* 91(3), 1542-1555.

Im, K., Avouac, J.P., Heimisson, E.R. & Elsworth, D., 2021. Ridgecrest aftershocks at Coso suppressed by thermal destressing, *Nature,* 595**,** 70.

Ross, Z. E., Idini, B., Zhe, J., Stephenson, O. L., Zhong, M., Xin, W., Zhan, Z., Simons, M., Fielding, E. J., Yun, S.-H., Hauksson, E., Moore, A. W., Liu, Z., Jung, J. (2019), Hierarchical interlocked orthogonal faulting in the 2019 Ridgecrest earthquake sequence, *Science*, 366, 346-351.

Stop 7: Lacy park (34.120389°N, 118.122357°W)

There are many faults that can be found in Los Angeles County. The closest one to Caltech is the Raymond Fault (or Raymond Hills Fault), a blind thrust fault. In 1988, it produced M_L 5.0 Pasadena earthquake with hypocenter underneath the northwestern corner of Caltech campus and knocked out powers from thousands of homes throughout Southern California. Paleoseismic studies from trenching have revealed at least 6 earthquakes with the most recent surface rupture occurring around 1050 CE and the oldest at least 41,500 years ago. The slip rate along the Raymond fault is poorly constrained and can range between 0.1 to 1.5 mm/yr. It has been estimated that the Raymond Fault can generate up to Mw 6.7 earthquake and could potentially coalesce with other connecting faults such as the Sierra Madre, the Eagle Rock-Verdugo, or the the Hollywood faults creating a much larger earthquake.

Lacy Park is located just on the footwall side of the Raymond Fault. The steep slope just north of the park is the scarp of the Raymond fault. There used to be a lake (Mission Lake, Kewen Lake, or Wilson lake with name changing based on the owner of the land) in the middle of the park (hence the namesake of the "Lake Avenue" in Pasadena) which was a sag pond.

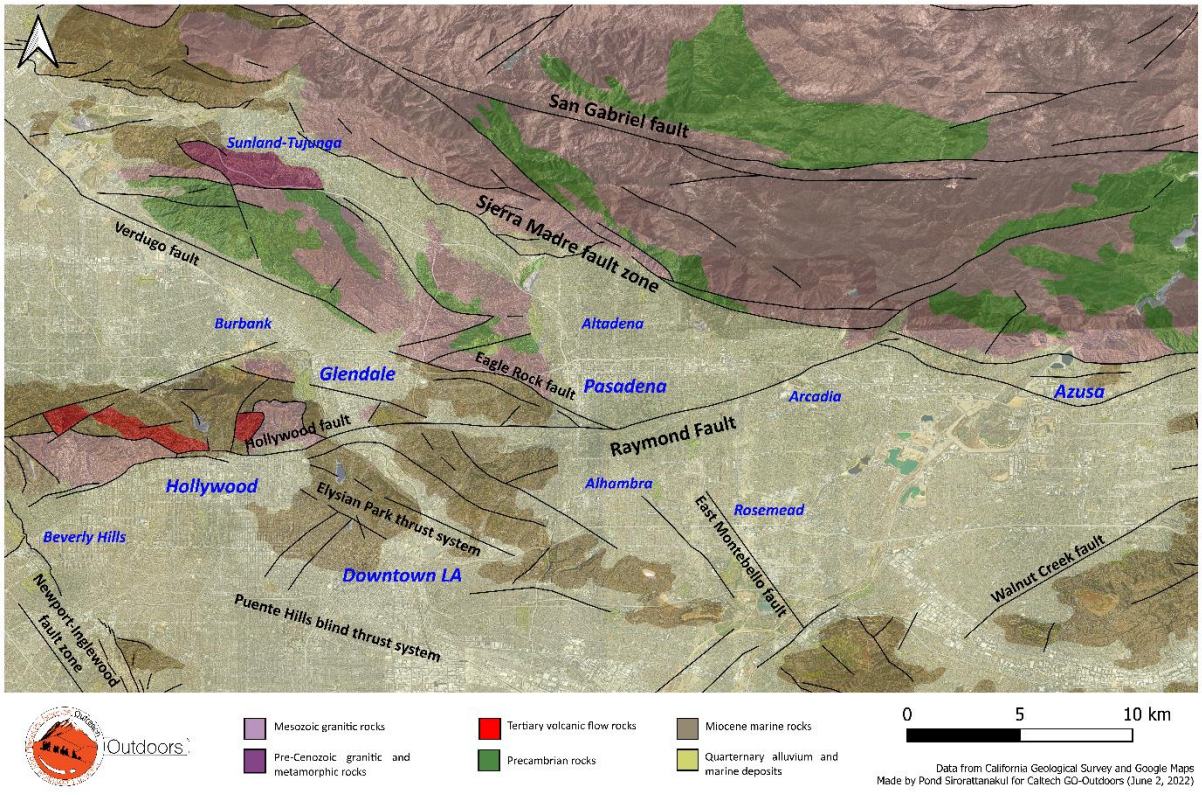

Figure 7.1. Geologic and faults map of the San Gabriel foothills.

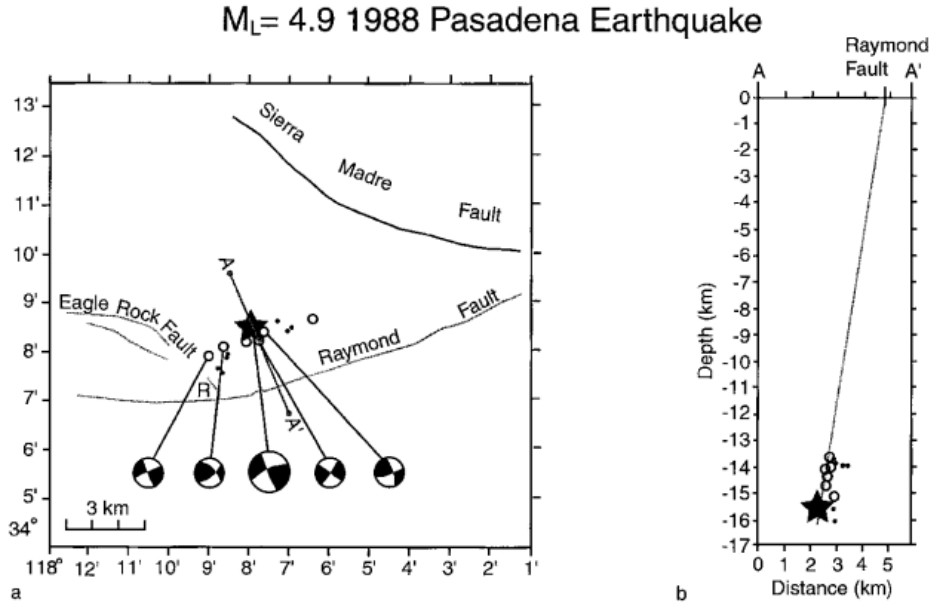

Figure 7.2. The 1988 Pasadena earthquake sequence. Figure is from Weaver and Dolan (2000).

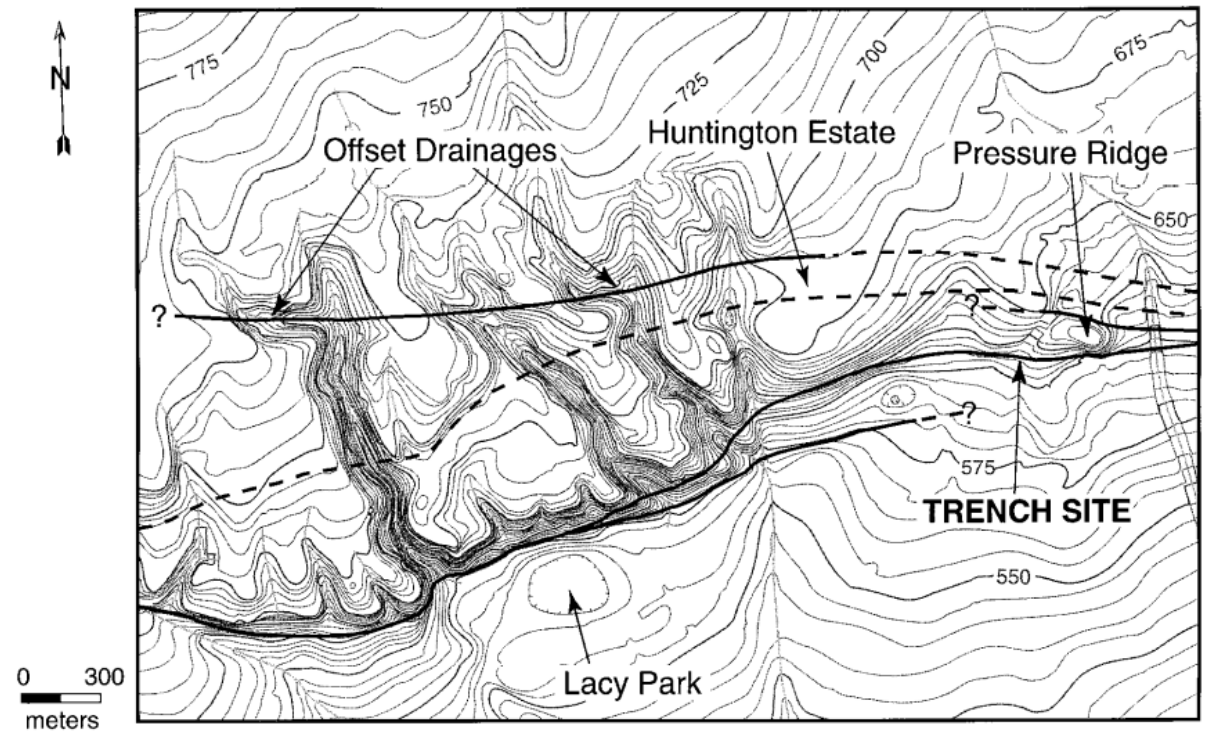

Figure 7.3. Contour map and geomorphic features associated with the Raymond Fault. Figure is from Weaver and Dolan (2000).

Faults can be found in our neighborhoods, all across the Los Angeles basin. Thrusting and folding associated to these accommodate NS contraction at a rate of nearly 1cm/yr of the LA basin. GNSS measurements of the ongoing contraction of the basin can be used to assess the seismic hazard. An example of a model of earthquake likelihood in the Los Angeles basin using seismological and geodetic observations is shown below.

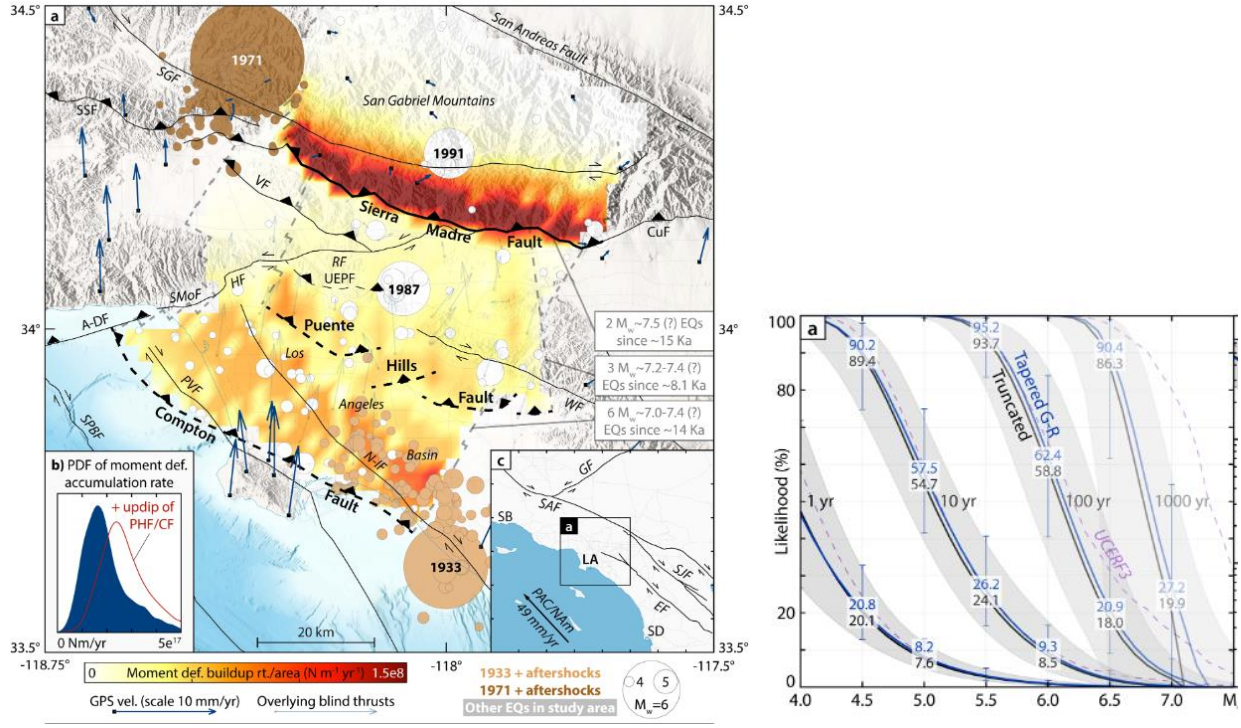

Figure 7.4. Moment deficit and earthquake likelihood in the Los Angeles basin. Figure is from Rollins and Avouac (2019).

Further readings

Jones, L. M., Sieh, K. E., Hauksson, E. & Hutton, K. L. (1990), The 3 December 1988 Pasadena, California earthquake: Evidence for strike-slip motion on the Raymond fault. *Bulletin of the Seismological Society of America*, 80(2), 474-482.

Rollins, C. & Avouac, J.-P. (2019), A geodesy- and seismicity-based local earthquake likelihood model for central Los Angeles, *Geophysical Research Letters*, 46, 3153-3162.

Weaver, K. D. & Dolan, J. F. (2000), Paleoseismology and Geomorphology of the Raymond Fault, Los Angeles County, California, *Bulletin of the Seismological Society of America*, 90(6), 1409-1429.